

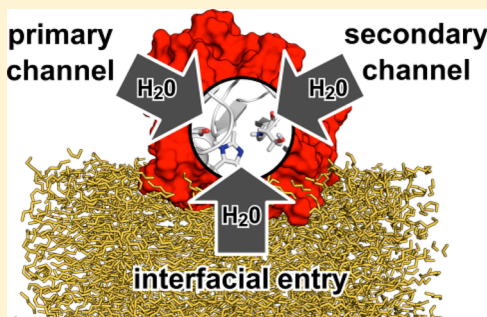
Solvent Flux Method (SFM): A Case Study of Water Access to *Candida antarctica* Lipase B

Sven P. Benson and Jürgen Pleiss*

Institute of Technical Biochemistry, University of Stuttgart, Allmandring 31, 70569 Stuttgart, Germany

 Supporting Information

ABSTRACT: The solvent flux method (SFM) was developed to comprehensively characterize the influx of solvent molecules from the solvent environment into the active site of a protein in the framework of molecular dynamics simulations. This was achieved by introducing a solvent concentration gradient as well as partially reorienting and rescaling the velocity vector of all solvent molecules contained within a spherical volume enclosing the protein, thus inducing an accelerated solvent influx toward the active site. In addition to the detection of solvent access pathway within the protein structure, it is hereby possible to identify potential amino acid positions relevant to solvent-related enzyme engineering with high statistical significance. The method is particularly aimed at improving the reverse hydrolysis reaction rates in nonaqueous media. *Candida antarctica* lipase B (CALB) binds to a triglyceride-water interface with its substrate entrance channel oriented toward the hydrophobic substrate interface. The lipase-triglyceride-water system served as a model system for SFM to evaluate the influx of water molecules to the active site. As a proof of principle for SFM, a previously known water access pathway in CALB was identified as the primary water channel. In addition, a secondary water channel and two pathways for water access which contribute to water leakage between the protein and the triglyceride-water interface were identified.



INTRODUCTION

Water molecules are directly involved in most enzymatic reactions. In hydrolysis reactions catalyzed by esterase and lipases (EC class 3.1) water acts as a nucleophile on an acyl-enzyme intermediate and thus facilitates the release of alcohol and acid constituents. While this natural degradative enzyme function is of substantial interest to a range of industrial applications¹ such as food processing, breaking down of natural materials, or waste treatment, significant strides have been made during the last decades to shift the chemical equilibrium toward the reverse synthesis reaction by transferring hydrolases into non-natural organic solvent environments^{2–4} or more recently ionic liquids.⁵ A broad range of substrates may thus be introduced to the reaction media as competing nucleophiles to the acyl-enzyme intermediate, which enables a diverse set of synthetic possibilities, such as transesterification, aminolysis, or thiolysis.^{2,4–6} Owing to the evolutionary adaptation of hydrolases to aqueous environments, transferring enzymes to anhydrous conditions raises new challenges like maintaining enzyme stability and optimizing the activity of the desired synthetic reaction. This is addressed by diverse avenues of biotechnological engineering, such as chemical modifications of enzyme surfaces,^{7–9} cross-linking,¹⁰ lyophilization¹¹ that exploits the phenomenon of pH memory,³ enzyme immobilization techniques,¹² engineering solvent conditions¹³ with appropriate log P values,¹⁴ or developing solvent tolerant variants by directed evolution.^{15,16} The presence of residual

hydration water is a prerequisite for enzyme activity in nonaqueous environments, which raises the fundamental problem of the desired reverse synthetic reaction competing with a undesired hydrolysis reaction.² Moreover, defining and maintaining dry conditions is difficult as well as costly to achieve on the industrial scale, which motivated Larsen et al.¹⁷ to propose an approach to suppress water as a nucleophile in *Candida antarctica* lipase B (CALB) by rationally designing variants that diminish the influx of water to the active site cavity and thus dramatically increase transacylation rates for vinyl butyrate over hydrolysis rates in butanol-water mixtures. CALB catalyzes hydrolysis of triglycerides in its native physiological setting; the natural substrate triglyceride is water-insoluble and forms phase-separated interfaces in aqueous environments, and thus CALB attaches to these interfaces in its active conformation, which is hereby oriented with its substrate channel toward the triglyceride phase.¹⁸ The most obvious water access pathway is thus considered to be blocked by the triglyceride which forms a hydrophobic barrier. However, a constant influx of water to the active site cavity is a prerequisite for hydrolysis to occur. Therefore, Larsen et al.¹⁷ proposed the existence of a water channel, which was targeted for mutation and implicitly validated by experiment. The aforementioned study supports the notion that a molecular understanding of the

Received: August 29, 2014

Published: October 7, 2014



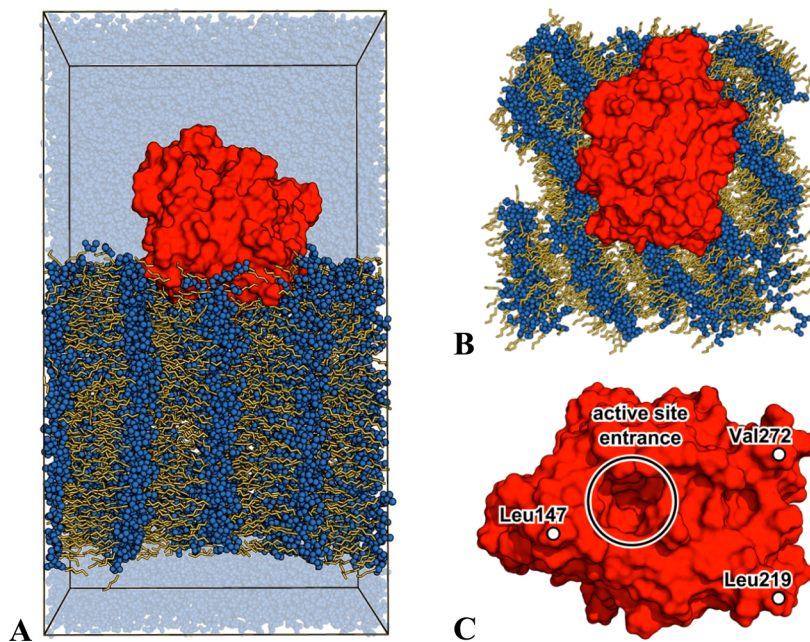


Figure 1. Simulation system consisting of *Candida antarctica* lipase B attached to a triglyceride-water interface (red surface: protein/dark blue spheres: polar triglyceride moieties/orange sticks: nonpolar triglyceride moieties) – A) Side view of full system including water (light blue spheres in the background)/B) Top view of protein and triglyceride layer/C) Bottom view of protein, white circle depicting the entrance to the active site, Leu147, Leu219, and Val272 are anchor residues by which CALB attaches to the triglyceride layer.¹⁸

role of residual water in nonaqueous reaction media is an integral part for furthering the development of hydrolase applications.⁴ Due to the difficulty of examining individual water molecules by experimental means, molecular dynamics (MD) studies have been conducted extensively to elucidate enzyme-solvent interactions under various conditions, which are comprehensively summarized in a recent review.¹⁹ Herein it is outlined how MD analysis on overall protein stability^{20–22} and flexibility^{23–25} in organic solvents or ionic liquids^{26,27} may offer deductions on mechanistic principles such as pH memory or the required minimal water content,²⁸ or even how significant parameters such as water activity may be modeled in a manner^{29,30} that is consistent with experimental data.³¹ By analyzing hydration water and its influence on protein secondary structure flexibility, it may also be possible to indirectly identify water entrance channels.³² In the present study, we propose an MD-based approach, the solvent flux method (SFM), which allows for a holistic characterization of the influx of solvent molecules through the protein structure and into the active site cavity. We hereby detect structural features relevant to the solvent influx, as well as positions that may prove beneficial to the rational design of enzyme variants for hydrolase applications. In this context, SFM was benchmarked for the influx of water molecules to the active site of CALB by comparing *in silico* predictions to the experimental results by Larsen et al.¹⁷

METHODS

Simulation Details. Molecular dynamics simulations were performed with the GROMACS 4.5.3^{33,34} software in an NPT ensemble at 298.15K and 1 bar, using the leapfrog integrator³⁵ with a time step of 2 fs. The Berendsen thermo- and barostats were applied for reasons of robustness and efficiency when converging systems far from equilibrium to the equilibrated state. This was deemed necessary since the SFM method introduces significant periodic rescaling and reorientation of

water molecule velocity vectors close to the protein and thus drives the systems out of equilibrium (see subsection ‘The Solvent Flux Method (SFM)’ for details). Water molecules with adjusted velocity vectors were relatively loosely coupled in intervals of 50 ps to prolong the velocity rescaling effect under Berendsen temperature coupling (Figures S9 and S10), while the remaining bulk water molecules, the triglyceride molecules, and the protein were coupled relatively tightly in intervals of 0.1 ps. To ensure that the structural integrity of the system remained intact during simulation, i.e. to avoid protein denaturation or distortions in the protein-triglyceride interface, position restraints with force constants of 1000 kJ mol⁻¹ nm⁻² were applied to the protein backbone and the triglyceride molecules in all spatial dimensions (Figure S7). To avoid artifacts due to position restraints under NPT conditions, the reference coordinates of each molecule group’s center of mass were rescaled periodically. Semi-isotropic pressure coupling was applied independently to the *x*–*y* plane and in *z*-dimension for a more accurate pressure representation of the planar triglyceride layer³⁶ in the model system. Pressure coupling intervals were set to 100 ps for the adjusted water molecules and to 5 ps for the protein, triglyceride, and bulk water molecules. The center of mass movements were removed every 100 simulation steps independently for all system components. Periodic boundary conditions were applied in all three dimensions. Hydrogen bonds were constrained with the LINCS algorithm.³⁷ Long-range electrostatics were calculated with the particle mesh Ewald (PME) method.^{38,39} Lennard-Jones interactions were treated with a cutoff and capped at 1.2 nm. The OPLS-AA all-atom force field⁴⁰ was used to parametrize the protein lipase B from *Candida antarctica* (CALB). Structural information on CALB was obtained from the Protein Data Bank (PDB: 1TCA⁴¹). Triglyceride molecules were parametrized with the Berger lipid model⁴² and the 1–4 interactions adapted with the half- ϵ double-pairlist method of Neale and Pomès⁴³ for consistency with the OPLS-AA force

field. Water molecules were parametrized with the TIP3P⁴⁴ model.

System Creation and Equilibration. A model system was created to mimic the conditions of the functionally active conformation of CALB at the triglyceride-water interface. As a prerequisite step, a random molecular arrangement of caproic (C6) triglyceride molecules and water molecules had to be equilibrated into a phase-separated triglyceride layer, in accordance to the approach proposed by Gruber et al.¹⁸ The resulting triglyceride-water interface hereby represents a model for the surface of large-scale aggregates in triglyceride in water emulsions (Figure 1). This model was deemed appropriate considering that the diameter of CALB (~5 nm) is 3 orders of magnitude smaller than experimentally determined triglyceride droplet diameters (~2.0 μm);⁴⁵ hence the droplet surface curvature is expected to be negligible on the model scale. Furthermore, when considering that the Coulomb potential decays with $1/r$, a layer thickness of ~7 nm should be sizable enough to ensure that the most significant Coulomb contributions to the nonbonded potential between the protein and the triglyceride surface are accounted for. Moreover, the lamellar-like nanostructures observed for the triglyceride layer model (Figure 1) are in agreement with previously published results on large-scale triglyceride aggregates⁴⁶ and our findings reported in a previous study.⁴⁷ The potential implication of these structural features on the mobility of water molecules are subject to a detailed follow-up study and will therefore not be elaborated on in this context. CALB was added to the triglyceride-water system and was attached to the layer with the active site entrance pointing toward the triglyceride phase, thus representing a model for the active binding configuration for triglyceride hydrolysis. The system was equilibrated for a further 500 ns, while monitoring protein adhesion and immersion depth (unpublished data).

The Solvent Flux Method (SFM). The design and benchmarking of SFM was tightly coupled to the test case system of protein CALB attached to the triglyceride-water interface and using water as the influx solvent. Two major technical considerations were formative for SFM during the design phase. First, it was considered necessary to differentiate solvent molecules that pass through a water access pathway into the active site cavity from other bulk solvent molecules. This was achieved in a recursive manner, by exploiting the fact that solvent molecules that are present within the active site cavity necessarily have to have passed through a water access pathway of the protein at a preceding point in time. It was thus possible to reconstruct solvent molecule pathways through the protein and therefore to detect general access pathways on a statistical basis. To identify such water molecules and to ensure that they had indeed passed into the active site cavity from the exterior, the water molecule closest to the reference atom at the intended influx site (here: oxygen atom of Ser105 of the catalytic triad of CALB) and within a spherical water removal cutoff of 0.35 nm was periodically removed from the simulation system after $\Delta t_{\text{ITER}} = 10 \text{ ps}$ (Figure 2). Not only did this ensure that after a given number of iterations all solvent molecules previously present within the active site cavity were evacuated, it also introduced an increased influx of solvent molecules due to the solvent concentration gradient between the active site of the protein and the exterior solvent bulk. Moreover, the removal of water served as a mechanistic model for water consumption during the native CALB hydrolysis reaction. The induced solvent influx ties in with the second major technical

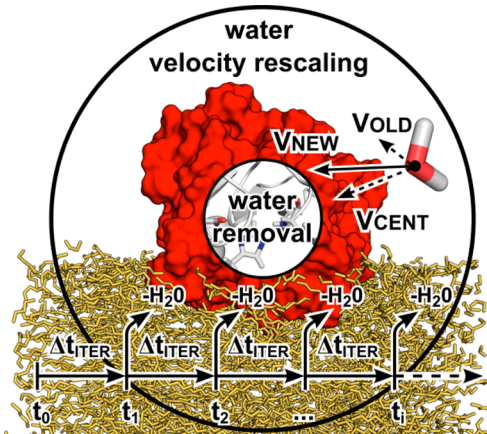


Figure 2. Velocity vector magnitudes of water molecules found within the water velocity rescaling cutoff around an active site reference atom are rescaled by a factor of v_{MULT} and then transformed to v_{NEW} after every iteration Δt_{ITER} . After every iteration Δt_{ITER} , a single water molecule is removed within the water removal cutoff radius. The direction of v_{NEW} is defined by X% of the rescaled magnitudes that are allocated to the original vector directions (v_{OLD}) and by Y% of the rescaled magnitudes that are allocated to the direction of the active site reference atom (V_{CENT}), whereby $X + Y = 100$ and $Y \gg X$.

consideration, which is the acceleration of conventional MD to rapidly overcome rate-limiting energy barriers specific to water influx and thus realize a significant data depth in a feasible duration of real-time. This was achieved by introducing a reorientation and rescaling of velocity vectors of water molecules that were located within a water velocity rescaling cutoff of 3 nm surrounding the active site reference, which was adjusted to incorporate the entirety of the protein and its first solvation shell. Within this cutoff, the velocity vectors of water molecules were periodically readjusted at constant time intervals Δt_{ITER} , simultaneously to the removal of water molecules. Velocity magnitudes of water molecules present within this cutoff were rescaled with a constant factor v_{MULT} , which effectively defines the strength of a periodic velocity pulse that is introduced to overcome the influx-rate-limiting energy barriers in a timely manner. The orientation of the new vectors was defined by assigning a fraction v_{OLD} of the respectively rescaled vector magnitudes to the unit vectors in the original direction, while a larger fraction $v_{\text{CENT}} = 100\% - v_{\text{OLD}}$ was assigned to unit vectors pointing toward the active site reference (Figure 2). Summation of these vector pairs yielded the new velocity vectors v_{NEW} , which were used to update the initial conditions at the beginning of an iteration. Thereafter, temperatures were allowed to converge back toward equilibrium during Δt_{ITER} . It proved necessary to additionally fine-tune the duration of this effect by modulating the temperature coupling parameter τ_{ITER} , thus coupling the velocity-adjusted water molecules more loosely than other system components. The process of single water molecule removal, velocity readjustment, and simulation continuation was repeated for a predefined number of iteration steps n_{ITER} . With ΔN_{WAT} denoting the sum of all water molecules removed during a full SFM run, it was thus possible to express the total water removal rate at the active site reference as $\Delta N_{\text{WAT}}/n_{\text{ITER}}$, with $\Delta N_{\text{WAT}}/n_{\text{ITER}} = 1$ signifying water removal at every iteration.

Table 1. Systematic Benchmarking of SFM Parameters v_{MULT} , v_{CENT} , τ_{ITER} , and Position Restraints (pos.res.) Was Conducted for $n_{\text{ITER}} = 100$ Iterations with Time Intervals of $\Delta t_{\text{ITER}} = 10$ ps, to Establish a Parameter Set That Maximizes the Water Removal Rate $\Delta N_{\text{WAT}}/n_{\text{ITER}}$

	variation of SFM parameters				$\Delta N_{\text{WAT}}/n_{\text{ITER}}$ 0.00–1.00	water removal rate at active site	structural integrity of protein and heat buildup in accelerated water			
	no.	v_{MULT}	pos. res. [kJ mol ⁻¹ nm ⁻²]	v_{CENT} [%]			RMSD ^a [nm]	ΔT_{ITER}^b [K]		
							0.00–1.00	0.03 ± 4.78		
velocity magnitude scaling	1	1.0	0	0	0.1	0.02	0.069 ± 0.002	0.03 ± 4.78		
	2	1.5	100	75	0.1	0.01	0.064 ± 0.003	0.04 ± 3.51		
	3	2.0	100	75	0.1	0.03	0.068 ± 0.003	0.77 ± 3.90		
	4	2.5	100	75	0.1	0.10	0.060 ± 0.006	0.31 ± 4.27		
	5	3.0	100	75	0.1	0.05	0.081 ± 0.007	0.63 ± 3.69		
	6	<u>3.5</u>	100	75	0.1	0.06	0.079 ± 0.008	0.77 ± 4.54		
position restraints	7	4.0	100	75	0.1	0.11	0.078 ± 0.009	1.16 ± 4.06		
	8	3.5	0	75	0.1	0.08	0.112 ± 0.012	0.00 ± 3.88		
	9	3.5	500	75	0.1	0.09	0.076 ± 0.003	0.71 ± 3.60		
	10	3.5	<u>1000</u>	75	0.1	0.14	0.059 ± 0.004	1.76 ± 4.13		
velocity vect. reorientation	11	3.5	5000	75	0.1	0.18	0.050 ± 0.001	0.99 ± 3.43		
	12	3.5	1000	0	0.1	0.07	0.060 ± 0.001	0.45 ± 3.71		
	13	3.5	1000	50	0.1	0.09	0.065 ± 0.002	0.84 ± 4.57		
	14	3.5	1000	<u>90</u>	0.1	0.16	0.069 ± 0.004	0.75 ± 4.44		
temperature coupling constant	15	3.5	1000	100	0.1	0.24	0.065 ± 0.005	0.23 ± 3.98		
	16	3.5	1000	90	0.5	0.40	0.067 ± 0.005	1.85 ± 4.88		
	17	3.5	1000	90	1	0.65	0.069 ± 0.005	4.32 ± 5.58		
	18	3.5	1000	90	5	0.55	0.081 ± 0.005	6.89 ± 8.57		
	19	3.5	1000	90	10	0.57	0.074 ± 0.006	4.10 ± 10.61		
	20	3.5	1000	90	25	0.73	0.070 ± 0.005	0.09 ± 10.83		
<u>21</u>	<u>3.5</u>	<u>1000</u>	<u>90</u>	<u>50</u>	<u>0.99</u>	<u>0.068 ± 0.004</u>	<u>0.60 ± 9.37</u>			
	22	3.5	1000	90	100	1.00	0.067 ± 0.004	10.21 ± 11.38		

^aRMSD after $n_{\text{ITER}} = 100$ iterations, averaged over $\Delta t_{\text{ITER}} = 10$ ps after backbone fitting to starting structure of $n_{\text{ITER}} = 1$. ^b $\Delta T_{\text{ITER}} = T_{100} - T_{10}$ of temperatures at $n_{\text{ITER}} = 100$ and $n_{\text{ITER}} = 10$, each averaged over $\Delta t_{\text{ITER}} = 10$ ps (largest s.d. shown); ΔT_{ITER} is a quantity to monitor whether accelerated molecules accumulate residual heat during SFM.

RESULTS

In this study, we present the computational solvent flux method (SFM) that was devised on the basis of nonequilibrium molecular dynamics (MD) simulations and comprehensively characterizes the access of solvent molecules from the bulk medium to the active site cavity of a protein. The intended purpose of SFM is thereby to identify solvent entrance pathways and moreover amino acid positions for solvent-related enzyme engineering, particularly in the context of improving reverse hydrolysis reaction rates. In the following, SFM and its parameters are thoroughly benchmarked in a case study of the enzyme *Candida antarctica* lipase B (CALB) with the solvent water (Figure 1). The feasibility of SFM analysis is then assessed by comparing simulation results with the successful experimental study of Larsen et al. on the same system,¹⁷ wherein enzyme variants were engineered that interfere with water access and thus increase transacylation versus hydrolysis rates.

SFM Parameter Optimization in the CALB-Triglyceride-Water System. The major parameters to configure SFM include the factor v_{MULT} by which velocity vectors of solvent molecules are rescaled, the temperature coupling constants τ_{ITER} of velocity-adjusted water molecules, the strength of position restraints (pos.res.) that are applied to the protein backbone as well as triglyceride molecules, and the percentage

v_{CENT} that defines the distribution of a rescaled velocity magnitude onto the vectors v_{OLD} and v_{CENT} (Figure 2 – details see the Methods section). These parameters were extensively tuned to attain a setup that balances the need for high water removal rates $\Delta N_{\text{WAT}}/n_{\text{ITER}}$ at the active site, while maintaining the structural integrity of the system despite the artificial forces introduced by SFM (Table 1). During parameter tuning, the root-mean-square deviation (RMSD) of the protein structure was monitored to assess the structural integrity of the system. The RMSD was calculated by fitting the protein backbone structure obtained after $n_{\text{ITER}} = 100$ iterations onto the initial protein structure. ΔT_{ITER} is defined as the temperature difference of the velocity-adjusted water molecules between iterations $n_{\text{ITER}} = 100$ and $n_{\text{ITER}} = 10$ ($\Delta T_{\text{ITER}} = |T_{100} - T_{10}|$) and was monitored to observe potential heat-buildup in the systems. T_{100} and T_{10} were thereby each averaged over the respective iteration duration of $\Delta t_{\text{ITER}} = 10$ ps (Table 1). No significant heat buildup was observed in any of the analyzed systems (Figures S4–S10). A system setup that corresponds to conventional MD simulation conditions without artificial external forces (Table 1 - system no. 1) served as a reference to compare systems tested during parameter tuning. As a first step, the velocity scaling factor v_{MULT} was varied from 1.5 to 4.0 (system no. 2–7), while the remaining parameters were initially set to position restraints of 100 kJ mol⁻¹ nm⁻², $v_{\text{CENT}} = 75\%$,

and $\tau_{\text{ITER}} = 0.1$ ps. Increasing v_{MULT} introduces the necessary energy to overcome barriers that water molecules would otherwise be unlikely to pass within $\Delta t_{\text{ITER}} = 10$ ps, as the low water removal rate $\Delta N_{\text{WAT}}/n_{\text{ITER}} = 0.02$ (system no. 1) demonstrates. While $\Delta N_{\text{WAT}}/\Delta t_{\text{ITER}}$ increased only slightly from initially 0.02 to 0.06, $v_{\text{MULT}} = 3.5$ (system no. 6) was maintained from thereon as a relatively high velocity rescaling factor in foresight of increasing $\Delta N_{\text{WAT}}/\Delta t_{\text{ITER}}$ via adjustment of the remaining parameters. The RMSD slightly increased to 0.079 nm (system no. 6), despite position restraints 100 kJ mol⁻¹ nm⁻². Therefore, position restraints were varied as a second step from 0 to 5000 kJ mol⁻¹ nm⁻² (system no. 8–11) to achieve a compromise between stable structures and conformational freedom of the protein backbone. Position restraints of 1000 kJ mol⁻¹ nm⁻² proved adequate in maintaining an RMSD of 0.059 nm (system no. 10) which was similar to the RMSD of the reference system (RMSD = 0.069 nm for system no. 1). As a third step, the amount of the rescaled water velocity magnitudes that is assigned to v_{CENT} was varied from 0 to 100% (system no. 12–15), which caused an increase of $\Delta N_{\text{WAT}}/\Delta t_{\text{ITER}}$ from 0.06 to 0.16 for $v_{\text{CENT}} = 90\%$. The RMSD = 0.069 nm (system no. 14) was thereby not significantly altered. A residual $v_{\text{OLD}} = 10\% = 100\% - v_{\text{CENT}}$ was maintained in the original vector directions to ensure residual sideways velocity components to laterally bypass potential barriers. The most significant increase in $\Delta N_{\text{WAT}}/\Delta t_{\text{ITER}}$ from 0.16 to 0.99 was obtained during the fourth parameter tuning step (system no. 16–22) by variation of the temperature coupling constant τ_{ITER} of the velocity-adjusted water molecules from 0.5 to 100 ps. The resulting final parameter set (system no. 21) of $v_{\text{MULT}} = 3.5$, pos.res. = 1000 kJ mol⁻¹ nm⁻², $v_{\text{CENT}} = 90\%$, and $\tau_{\text{ITER}} = 50$ ps ensured the removal of water after nearly every iteration with $\Delta N_{\text{WAT}}/\Delta t_{\text{ITER}} = 0.99$, while maintaining the structural integrity of the system with RMSD = 0.059 nm and without heating artifacts due to velocity adjustment.

Identifying Water Access Pathways with SFM in the CALB-Triglyceride-Water System. SFM was applied to test for water influx in the system of CALB attached to a triglyceride-water interface (Figure 1), using the parameter set as optimized in the previous section. Influx occurred toward the active site reference oxygen atom of Ser105 of CALB, due to the water concentration gradient between the protein exterior and the active site, induced by the periodic removal of water molecules and the periodic introduction of a radial velocity pulse to the water molecules in close proximity to the protein. After an iteration $n_{\text{EVAC}} = 100$, it was ensured that all water molecules that were originally present in the active site cavity had been removed, and thus any water molecules that were consecutively removed in $n_i > n_{\text{EVAC}}$ necessarily had to have passed through a water access pathway of the protein to reach the active site. The pathway of any water molecule that was thus removed during an iteration n_p with $n_{\text{EVAC}} < n_p < n_{\text{ITER}} = 500$, was reconstructed by superimposing the system coordinates in a least-square fit of protein backbone atoms of all prior iterations $n_j < n_p$. Moreover, the contact frequency between the removed water molecules and all amino acids was evaluated on the basis of the reconstructed water pathways by counting the number of iterations during which a water molecule was found within the contact distance $r_{\text{HSPOT}} = 0.4$ nm to a specific amino acid. The SFM analysis was applied to three different initial conformations of the model system (Figure 1) which were derived from a prior 100 ns MD

simulation under conventional equilibrium conditions without external forces or water removal (Figure S1), whereby the starting coordinates corresponded to the minimal, the maximal, and an average RMSD value of the CALB protein backbone. For each initial conformation, SFM was performed 50 times for a total of 150 independent runs, each consisting of 500 iterations of $\Delta t_{\text{ITER}} = 10$ ps, amounting to a total of 750 ns of accelerated SFM analysis. Contact frequencies were extracted from this data set, normalized, and merged for a holistic and statistically significant representation of probable water access pathways during influx to the active site cavity of CALB. Amino acid positions corresponding to increased contact frequencies were defined as hotspot areas H1–H9 (Figure 3).

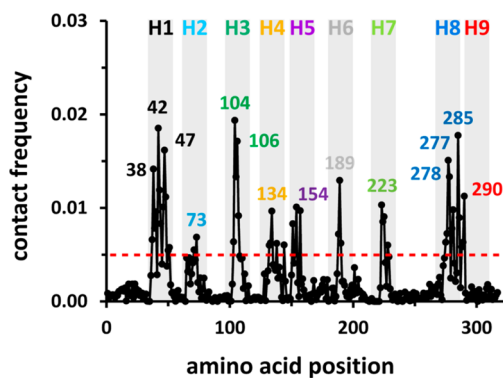


Figure 3. Contact frequency between influx water and position-specific amino acid are presented as the number of observed water contacts relative to all evaluated system conformations of the SFM analysis (all potential contacts). Hotspot areas H1–H9 were defined as peaks greater than a contact frequency cutoff value (red dotted line) and were arbitrarily colored for reasons of easy distinction and reference in Table 2 and Figure 4. Single positions that correspond to the highest values of the hotspot areas were labeled and defined as hotspot positions.

Individual hotspot positions (Table 2) contained in hotspot areas were defined on the basis of their contact frequency, their relative position within the CALB structure (Figure 4A), and by visualizing reconstructed water influx pathways (Figure 4B). Hotspot positions were thereby predominantly found in close proximity to the triglyceride-water interface (Figure 1). Positions Thr42/Ser47 of H1 and Gln106 of H3 coincide with the mutational strategy on CALB of Larsen et al.,¹⁷ who proposed and implicitly validated a water channel at these exact positions. Because it had the highest relative contact frequency (Table 2), we refer to this channel as the primary water channel (PWC). Three additional potential water access pathways with high relative contact frequencies were identified, the secondary water channel (SWC) at position Val134 of H4 and two interfacial water entrances IWE1 and IWE2 at position Asp223 of H7 and Lys290 of H9, respectively, which feature polar residues on the protein surface and are in immediate contact with the triglyceride interface. IWE1 and IWE2 are therefore considered to potentially contribute to the significant water influx through the substrate channel leading from the triglyceride interface to the active site (Figure 4B), which is lined by positions Val154 of H5, Ile189 of H6, and Leu278/Ile285 of H8. Other potential hotspot positions, such as Pro38 of H1, Leu73 of H2, and Leu277 of H8, were estimated to be potential barriers. Their increased contact frequency was

Table 2. Compiled Hotspot Areas H1–H9 Obtained from 150 SFM Runs Analyzing Water Influx into CALB Attached to a Triglyceride-Water Interface Depicted in Figure 1^a

	pos.	AA	property	rel. freq.	d_{act} [Å]	positioning	Assessment	chan
H1	38	PRO	hphob	0.71	5.7	periphery	adjacent to primary water channel	-
	42	THR	hphil	1.00	7.8	periphery	primary water channel	PWC
	47	SER	hphil	0.85	8.5	periphery	primary water channel	PWC
H2	73	LEU	hphob	0.27	10.8	surface	probable barrier, adjacent to Lys290	-
H3	104	TRP	hphob	0.96	4.8	active site	active site	-
	106	GLN	hphil	0.98	4.8	active site	primary water channel	PWC
H4	134	ASP	neg	0.54	11.5	periphery	potential secondary water channel	SWC
H5	154	VAL	hphob	0.56	12.0	periphery	entrance substrate channel	-
H6	189	ILE	hphob	0.96	9.4	surface	entrance substrate channel	-
H7	223	ASP	neg	0.65	12.7	surface	potential interfacial water entrance	IWE1
	277	LEU	hphob	0.77	8.7	periphery	probable barrier, adj. to Asp223 and Ser47	
H8	278	LEU	hphob	0.88	6.9	periphery	entrance substrate channel	
	285	ILE	hphob	0.94	11.3	periphery	entrance substrate channel	
H9	290	LYS	pos	0.52	17.7	surface	potential interfacial water entrance	IWE2

^aData shown includes amino acid positions (pos.), amino acids (AA), amino acid properties in regards to charge and hydrophobicity/-philicity (property), the relative contact frequency calculated by SFM (rel. freq.), the distance (d_{act}) of residue Cα carbon atoms relative to the oxygen reference atom of Ser105 at the active site, the spatial positioning of the amino acid in the protein structure (positioning), a general assessment of the individual hotspot positions (assessment) and a channel definition (chan), whereby PWC is the water channel reported by Larsen et al., SWC a potential secondary water channel and IWE1/IWE2 potential water entrances located at the protein-triglyceride interface that may contribute to the water influx via the substrate channel.

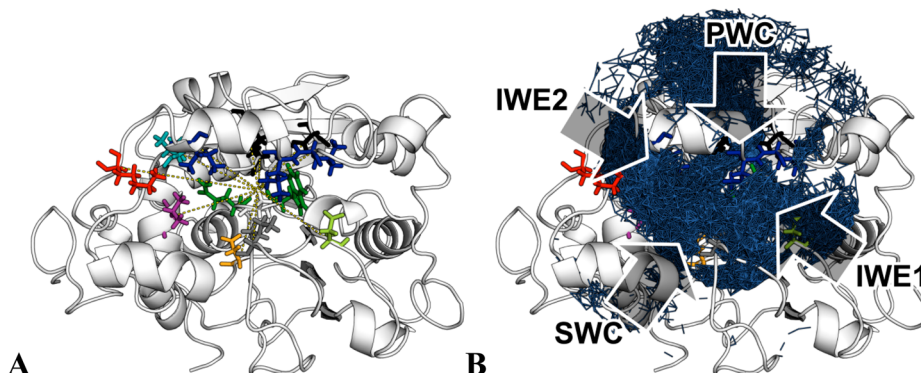


Figure 4. (A) Hotspot positions in the CALB protein structure with colors corresponding to H1–H9 of Figure 3, dotted lines point toward the active site Ser105, protein is represented in the bottom view, i.e. from the perspective of the triglyceride-water interface that CALB is attached to (see Figure 1) (B) Water influx pathways from five full SFM runs of 500 iterations length are superimposed onto the same depiction as part (A) to illustrate potential water access pathways (arrows). Helices between the PWC and SWC channels and the triglyceride layer stop water “leakage” in between the protein and the interface, whereas IWE1 and IWE2 significantly contribute to the influx via the substrate channel, which is situated in the central part of the protein in both depictions.

attributed to their close proximity to a water access pathway or in the case of Trp104 of H3 to Ser105.

PWC was identified as the most frequented water access pathway (Figure 5A and Table 2). Even residue Gln46, which was defined as the outer entrance in the study of Larsen et al.,¹⁷ was resolved by SFM (Figure 3). Water influx via PWC occurred in the loop region between $\alpha 5$ and $\beta 2$, according to the secondary structure numbering by Uppenberg et al.⁴¹ (Figure 5A). Access to channel SWC (Figure 5B) occurred in the loop region between $\alpha 5$ and $\beta 5$, which is located in close proximity to the catalytically active Ser105 and is structurally slightly submerged relative to the protein surface, yet fully solvent accessible between $\alpha 7$ and the loop region between $\beta 6$ and $\beta 7$. Access to entrance IWE1 (Figure 5C), which is located directly at the boundary between CALB and the triglyceride layer, occurred at the loop preceding $\alpha 9$, which was slightly denatured at its N-terminus due to the direct interaction with the triglyceride layer. IWE1 may thus contribute to the influx of water via the triglyceride layer and through the substrate channel, as water molecules were observed to “leak” in between

the protein and the triglyceride layer (Figure 4B). Access to entrance IWE2 (Figure 5D) occurred in the loop region between $\beta 8$ and $\beta 9$ close to the C-terminus of CALB, which also directly borders the triglyceride-water interface and can thus potentially also contribute to the interfacial leakage.

DISCUSSION

Water Influx to the Active Site of CALB Modeled by SFM. Results from SFM suggest that the triglyceride layer, which the enzyme CALB is attached to in its catalytically active conformation (Figure 1), does not constitute a hydrophobic barrier that excludes water molecules from entering the enzyme via the buried substrate channel. On the contrary, significant interfacial leakage between the protein and the triglyceride interface was observed (Figure 4B) that is comparable in significance to the water influx via the known primary water channel PWC¹⁷ and higher than the influx via the potential secondary channel SWC identified by SFM (Table 2). The fact that during equilibration of the protein-triglyceride system the

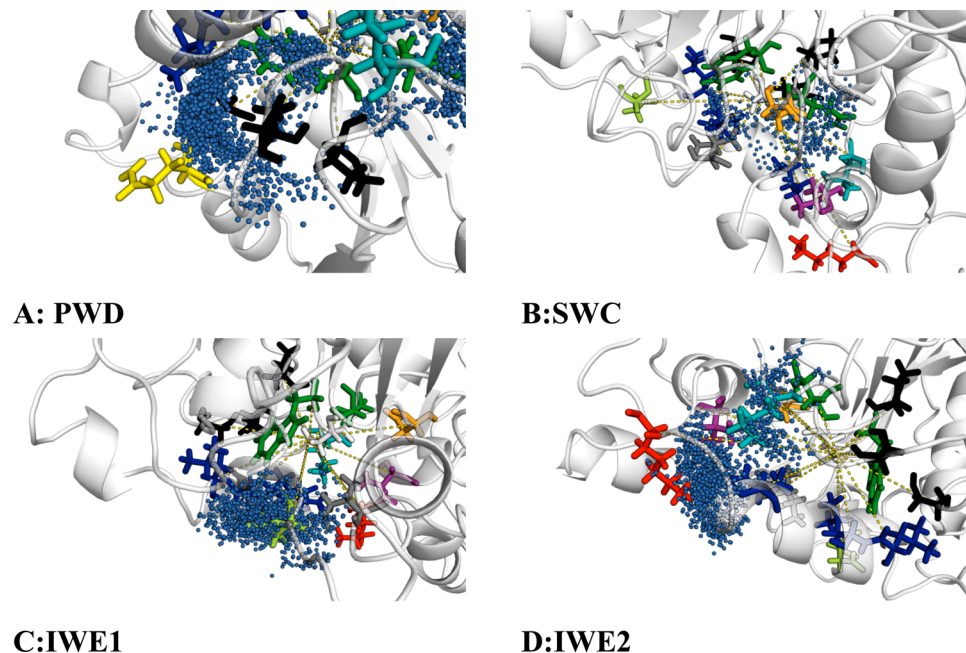


Figure 5. Water influx to CALB attached to a triglyceride-water interface (Figure 1), dotted lines point toward the catalytically active Ser105. (A) The outer PWC channel entrance is defined by Gln46 (yellow sticks) and the residues Thr42/Ser47 (middle black sticks). (B) Channel SWC is defined by Asp134 (orange) as a potential water entrance in close proximity to Ser105. (C) Entrance IWE1 (light green) is defined by Asp223 and is located at the triglyceride-water interface and may thus contribute to interfacial leakage of water. (D) Entrance IWE2 (light green) is defined by Lys290 and is located at the triglyceride-water interface and may thus also contribute to interfacial leakage of water.

protein immersed into the triglyceride layer (Figure S1B) implies that the observed interfacial water leakage is not a consequence of incomplete protein adsorption in the model. The origins of the interfacial water leakage is instead accredited to the self-association structures of polar triglyceride moieties that are formed in aggregates at equilibrium.⁴⁷ Lamellar-like self-association structures might therefore serve as a polar microenvironment that can facilitate an influx of water molecules through the interface and into the active site via the substrate channel. In this regard, the polar amino acids of IWE1 and IWE2 are potential avenues for water access through the protein-triglyceride-water interface (Figure 6). These considerations are subject of an ongoing study to clarify the involvement of triglyceride molecule association on interfacial water, where the quality of the interfacial model is placed under particular scrutiny.

SFM Modeling Quality and Applicability. It was demonstrated that the solvent flux method (SFM) presented in this study is able to successfully identify solvent access pathways in proteins, by revealing the primary water channel (PWC) and other key positions in CALB that may increase synthesis versus hydrolysis in nonaqueous media when appropriately mutated, as demonstrated by Larsen et al.¹⁷ Although SFM introduces artificial external forces to MD simulations by the periodic velocity adjustment of water molecules and may thus raise concerns about misleading biases, one must consider the limitations of conventional MD in sampling rare events such as the passage of a molecule through a channel, both in real and computational time. This is particularly difficult when seeking to simultaneously model multiple rare events. Due to the limitations of computational resources, exploring complex problems such as the solvent flux through an enzyme with significant statistics is currently not feasible by conventional MD approaches. Therefore, increasing

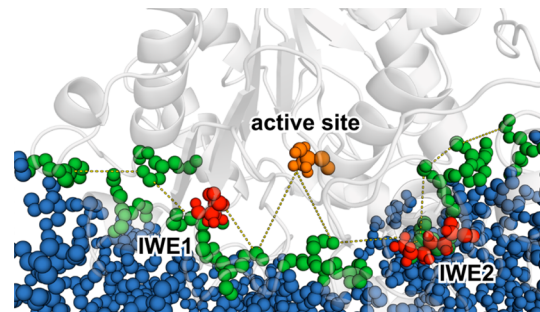


Figure 6. Interfacial leakage of water in between the protein (gray cartoon) and the triglyceride-water interface. Depiction of two hypothetical water influx pathways (dotted lines) through the triglyceride layer. In the model, water influx was found to occur via the submerged entrance to the active site (orange spheres: catalytically active Ser105). In this context, water influx may be mediated by polar triglyceride moieties (blue spheres), particular polar moieties in close contact with the protein (green spheres). IWE1 and IWE2 (red spheres), which are polar amino acid residues of CALB in direct contact with the triglyceride-water interface, are proposed to assist in mediating the influx of water molecules through the triglyceride-water interface.

the sampling efficiency of molecular dynamics by introducing biases to the potential function to overcome energy barriers has become a widely used strategy, such as accelerated molecular dynamics (AMD),⁴⁸ replica-exchange molecular dynamics (REMD),⁴⁹ steered molecular dynamics (SMD),⁵⁰ or random acceleration molecular dynamics (RAMD).⁵¹ The multitude of successful applications and insights attained by these methods is testament to their usefulness in studying biophysical effects that would otherwise be inaccessible. In this context, SFM offers the means to rapidly and comprehensively sample solvent flux behavior throughout a protein, which allows for an

atomistic resolution of structural features and positions that are relevant to enzyme-solvent interactions. It is thereby unique in its approach of simultaneously modeling the accelerated influx of multiple solvent molecules that randomly come into contact with the protein from the solvent bulk and to extract meaningful data in form of contact frequencies and compiled pathways of individual water molecules during influx. In this regard, other comparable methods are either less deliberate in overcoming specific energy barriers,^{48,49} are restricted to single molecules and predefined geometric reaction coordinates,⁵⁰ or are more suited to resolving the efflux of single substrates.⁵¹ SFM holds the potential of exploring solvent-enzyme interactions beyond the hydration-related context,^{21,22,24,26,27,52} which seems to be required, considering that identifying the role of residual water in facilitating enzyme activity in nonaqueous synthetic hydrolase applications has proven to be nontrivial.⁵³ Even studies on “dry” systems have shown that residual water is in fact not restricted to the hydration of proteins but instead partitions into the solvent environment under equilibrium conditions.⁵⁴ Understanding the behavior of residual free water in reaction media may thus prove particularly useful for synthetic hydrolase applications in nonaqueous environments,⁴ specifically to eliminate water as a competing nucleophile. SFM in conjunction with the desired organic nucleophile may additionally benefit enzyme engineering in improving synthesis reactions by rational design. In principle, SFM can thereby aid in resolving the competition between synthesis and degradation, which remains a fundamental problem of designing a particular hydrolase application and is difficult to overcome without a deeper mechanistic understanding of molecular solvent fluxes.

■ ASSOCIATED CONTENT

Supporting Information

Additional information concerning system equilibration, statistics for the contact frequency analysis and graphs complementing SFM parameter optimization for the CALB and water test system. This material is available free of charge via the Internet at <http://pubs.acs.org>.

■ AUTHOR INFORMATION

Corresponding Author

*Phone: +49 71168563191. E-mail: Juergen.Pleiss@itb.uni-stuttgart.de.

Notes

The authors declare no competing financial interest.

■ ACKNOWLEDGMENTS

We would like to thank the German Research Foundation (DFG) for financial support of the project within the Cluster of Excellence in Simulation Technology (EXC 310/1) at the University of Stuttgart. We thank the high performance computing center Stuttgart (HLRS) for their support and for supplying the computational resources.

■ REFERENCES

- (1) Panda, T.; Gowrishankar, B. S. Production and Applications of Esterases. *Appl. Microbiol. Biotechnol.* **2005**, *67*, 160–169.
- (2) Gupta, M. N.; Roy, I. Enzymes in Organic Media. *Eur. J. Biochem.* **2004**, *271*, 2575–2583.
- (3) Zaks, A.; Klibanov, A. M. Enzymatic Catalysis in Nonaqueous Solvents. *J. Biol. Chem.* **1988**, *263*, 3194–3201.

- (4) Hudson, E. P.; Eppler, R. K.; Clark, D. S. Biocatalysis In Semiaqueous and Nearly Anhydrous Conditions. *Curr. Opin. Biotechnol.* **2005**, *16*, 637–643.
- (5) van Rantwijk, F.; Sheldon, R. A. Biocatalysis in Ionic Liquids. *Chem. Rev.* **2007**, *107*, 2757–2785.
- (6) Schmid, A.; Dordick, J. S.; Hauer, B.; Kiener, A.; Wubbolt, M.; Witholt, B. Industrial Biocatalysis Today and Tomorrow. *Nature* **2001**, *409*, 258–268.
- (7) Distel, K. A.; Zhu, G. Y.; Wang, P. Biocatalysis Using an Organic-Soluble Enzyme for the Preparation of Poly(Lactic Acid) in Organic Solvents. *Bioresour. Technol.* **2005**, *96*, 617–623.
- (8) Mine, Y.; Zhang, L.; Fukunaga, K.; Sugimura, Y. Enhancement of Enzyme Activity and Enantioselectivity by Cyclopentyl Methyl Ether in the Transesterification Catalyzed by Pseudomonas Cepacia Lipase Co-Lyophilized with Cyclodextrins. *Biotechnol. Lett.* **2005**, *27*, 383–388.
- (9) Jiang, Y.; Dalton, H. Chemical Modification of the Hydroxylase of Soluble Methane Monooxygenase Gives One Form of the Protein with Significantly Increased Thermostability and Another That Functions Well in Organic-Solvents. *Biochim. Biophys. Acta, Gen. Subj.* **1994**, *1201*, 76–84.
- (10) Govardhan, C. P. Crosslinking of Enzymes for Improved Stability and Performance. *Curr. Opin. Biotechnol.* **1999**, *10*, 331–335.
- (11) Lindsay, J. P.; Clark, D. S.; Dordick, J. S. Combinatorial Formulation of Biocatalyst Preparations for Increased Activity in Organic Solvents: Salt Activation of Penicillin Amidase. *Biotechnol. Bioeng.* **2004**, *85*, 553–560.
- (12) Persson, M.; Wehtje, E.; Adlercreutz, P. Factors Governing the Activity of Lyophilised and Immobilised Lipase Preparations in Organic Solvents. *ChemBioChem* **2002**, *3*, 566–571.
- (13) Wescott, C. R.; Klibanov, A. M. The Solvent Dependence of Enzyme Specificity. *Biochim. Biophys. Acta, Protein Struct. Mol. Enzymol.* **1994**, *1206*, 1–9.
- (14) Laane, C. Medium-Engineering For Bio-Organic Synthesis. *Biocatal. Biotransform.* **1987**, *1*, 17–22.
- (15) Bornscheuer, U. T.; Pohl, M. Improved Biocatalysts by Directed Evolution and Rational Protein Design. *Curr. Opin. Chem. Biol.* **2001**, *5*, 137–143.
- (16) Cirino, P. C.; Arnold, F. H. Protein Engineering of Oxygenases for Biocatalysis. *Curr. Opin. Chem. Biol.* **2002**, *6*, 130–135.
- (17) Wittrup Larsen, M.; Zielinska, D. F.; Martinelle, M.; Hidalgo, A.; Jensen, L. J.; Bornscheuer, U. T.; Hult, K. Suppression of Water as a Nucleophile in *Candida antarctica* Lipase B Catalysis. *ChemBioChem* **2000**, *11*, 796–801.
- (18) Gruber, C. C.; Pleiss, J. Lipase B from *Candida Antarctica* Binds to Hydrophobic Substrate-Water Interfaces via Hydrophobic Anchors Surrounding the Active Site Entrance. *J. Mol. Catal. B: Enzym.* **2012**, *84*, 48–54.
- (19) Lousa, D.; Baptista, A. M.; Soares, C. M. A Molecular Perspective on Nonaqueous Biocatalysis: Contributions from Simulation Studies. *Phys. Chem. Chem. Phys.* **2013**, *15*, 13723–13736.
- (20) Tejo, B.; Salleh, A.; Pleiss, J. Structure and Dynamics of *Candida rugosa* Lipase: the Role of Organic Solvent. *J. Mol. Model.* **2004**, *10*, 358–366.
- (21) Soares, C. M.; Teixeira, V. H.; Baptista, A. M. Protein Structure and Dynamics in Nonaqueous Solvents: Insights from Molecular Dynamics Simulation Studies. *Biophys. J.* **2003**, *84*, 1628–1641.
- (22) Norin, M.; Haeffner, F.; Hult, K.; Edholm, O. Molecular Dynamics Simulations of an Enzyme Surrounded by Vacuum, Water, or a Hydrophobic Solvent. *Biophys. J.* **1994**, *67*, 548–559.
- (23) Rehm, S.; Trodler, P.; Pleiss, J. Solvent-Induced Lid Opening in Lipases: A Molecular Dynamics Study. *Protein Sci.* **2010**, *19*, 2122–2130.
- (24) Micalo, N. M.; Soares, C. M. Modeling Hydration Mechanisms of Enzymes in Nonpolar and Polar Organic Solvents. *FEBS J.* **2007**, *274*, 2424–2436.
- (25) Trodler, P.; Schmid, R. D.; Pleiss, J. Modeling of Solvent-Dependent Conformational Transitions in *Burkholderia cepacia* Lipase. *BMC Struct. Biol.* **2009**, *9*.

- (26) Klähn, M.; Lim, G. S.; Seduraman, A.; Wu, P. On the Different Roles of Anions and Cations in the Solvation of Enzymes in Ionic Liquids. *Phys. Chem. Chem. Phys.* **2011**, *13*, 1649–1662.
- (27) Micaelo, N. M.; Baptista, A. M.; Soares, C. M. Parametrization of 1-Butyl-3-methylimidazolium Hexafluorophosphate/Nitrate Ionic Liquid for the GROMOS Force Field. *J. Phys. Chem. B* **2006**, *110*, 14444–14451.
- (28) Affleck, R.; Xu, Z. F.; Suzawa, V.; Focht, K.; Clark, D. S.; Dordick, J. S. Enzymatic Catalysis and Dynamics in Low-Water Environments. *Proc. Natl. Acad. Sci. U.S.A.* **1992**, *89*, 1100–1104.
- (29) Branco, R. J. F.; Gruber, M.; Denis, V.; Pleiss, J. Molecular Mechanism of the Hydration of *Candida antarctica* Lipase B in the Gas Phase: Water Adsorption Isotherms and Molecular Dynamics Simulations. *ChemBioChem* **2009**, *10*, 2913–2919.
- (30) Wedberg, R.; Abildskov, J.; Peters, G. H. Protein Dynamics in Organic Media at Varying Water Activity Studied by Molecular Dynamics Simulation. *J. Phys. Chem. B* **2012**, *116*, 2575–2585.
- (31) Valivety, R. H.; Halling, P.; Macrae, A. R. Reaction Rate with Suspended Lipase Catalyst Shows Similar Dependence on Water Activity in Different Organic Solvents. *Biochim. Biophys. Acta, Protein Struct. Mol. Enzymol.* **1992**, *1118*, 218–222.
- (32) Bös, F.; Pleiss, J. Multiple Molecular Dynamics Simulations of TEM beta-Lactamase: Dynamics and Water Binding of the omega-Loop. *Biophys. J.* **2009**, *97*, 2550–2558.
- (33) Hess, B.; Kutzner, C.; van der Spoel, D.; Lindahl, E. GROMACS 4: Algorithms for Highly Efficient, Load-Balanced, and Scalable Molecular Simulation. *J. Chem. Theory Comput.* **2008**, *4*, 435–447.
- (34) van der Spoel, D.; Lindahl, E.; Hess, B.; Groenhof, G.; Mark, A. E.; Berendsen, H. J. C. GROMACS: Fast, Flexible, and Free. *J. Comput. Chem.* **2005**, *26*, 1701–1718.
- (35) Wensink, E. J. W.; Hoffmann, A. C.; van Maaren, P. J.; van der Spoel, D. Dynamic Properties of Water/Alcohol Mixtures Studied by Computer Simulation. *J. Chem. Phys.* **2003**, *119*, 7308–7317.
- (36) Marrink, S. J.; Mark, A. E. Effect of Undulations on Surface Tension in Simulated Bilayers. *J. Phys. Chem. B* **2001**, *105*, 6122–6127.
- (37) Ryckaert, J. P.; Ciccotti, G.; Berendsen, H. J. C. Numerical-integration of Cartesian Equations of Motion of a System with Constraints - Molecular-Dynamics of n-Alkanes. *J. Comput. Phys.* **1977**, *23*, 327–341.
- (38) Essmann, U.; Perera, L.; Berkowitz, M. L.; Darden, T.; Lee, H.; Pedersen, L. G. A Smooth Particle Mesh Ewald Method. *J. Chem. Phys.* **1995**, *103*, 8577–8593.
- (39) York, D. M.; Darden, T. A.; Pedersen, L. G. The Effect of Long-Range Electrostatic Interactions in Simulations of Macromolecular Crystals - a Comparison of the Ewald and Truncated List Methods. *J. Chem. Phys.* **1993**, *99*, 8345–8348.
- (40) Jorgensen, W. L.; Maxwell, D. S.; TiradoRives, J. Development And Testing Of The OPLS All-Atom Force Field On Conformational Energetics And Properties Of Organic Liquids. *J. Am. Chem. Soc.* **1996**, *118*, 11225–11236.
- (41) Uppenberg, J.; Hansen, M. T.; Patkar, S.; Jones, T. A. The Sequence, Crystal Structure Determination and Refinement of Two Crystal Forms of Lipase B from *Candida Antarctica*. *Structure* **1994**, *2*, 293–308.
- (42) Berger, O.; Edholm, O.; Jähnig, F. Molecular Dynamics Simulations of a Fluid Bilayer of Dipalmitoylphosphatidylcholine at Full Hydration, Constant Pressure, and Constant Temperature. *Biophys. J.* **1997**, *72*, 2002–2013.
- (43) Neale, C.; Pomès, R. Combination rules for united-atom lipids and OPLS-AA proteins, This unpublished document is available online from the Pomès lab at <http://www.pomeslab.com/files/lipidCombinationRules.pdf>. (accessed August 1, 2013).
- (44) Jorgensen, W. L.; Chandrasekhar, J.; Madura, J. D.; Impey, R. W.; Klein, M. L. Comparison of simple potential functions for simulating liquid water. *J. Chem. Phys.* **1983**, *79*, 926–935.
- (45) Jurado, E.; Camacho, F.; Luzón, G.; Fernández-Serrano, M.; García-Román, M. Kinetic Model for the Enzymatic Hydrolysis of Tributyrin in O/W Emulsions. *Chem. Eng. Sci.* **2006**, *61*, 5010–5020.
- (46) Sum, A. K.; Biddy, M. J.; de Pablo, J. J.; Tupy, M. J. Predictive Molecular Model for the Thermodynamic and Transport Properties of Triacylglycerols. *J. Phys. Chem. B* **2003**, *107*, 14443–14451.
- (47) Benson, S. P.; Pleiss, J. Molecular Dynamics Simulations of Self-Emulsifying Drug-Delivery Systems (SEDDS): Influence of Excipients on Droplet Nanostructure and Drug Localization. *Langmuir* **2014**, *30*, 8471–8480.
- (48) Hamelberg, D.; Mongan, J.; McCammon, J. A. Accelerated Molecular Dynamics: A Promising and Efficient Simulation Method for Biomolecules. *J. Chem. Phys.* **2004**, *120*, 11919–11929.
- (49) Sugita, Y.; Okamoto, Y. Replica-Exchange Molecular Dynamics Method for Protein Folding. *Chem. Phys. Lett.* **1999**, *314*, 141–151.
- (50) Lu, H.; Isralewitz, B.; Krammer, A.; Vogel, V.; Schulten, K. Unfolding of Titin Immunoglobulin Domains by Steered Molecular Dynamics Simulation. *Biophys. J.* **1998**, *75*, 662–671.
- (51) Lüdemann, S. K.; Lounnas, V. r.; Wade, R. C. How Do Substrates Enter and Products Exit the Buried Active Site of Cytochrome P450cam? 1. Random Expulsion Molecular Dynamics Investigation of Ligand Access Channels and Mechanisms. *J. Mol. Biol.* **2000**, *303*, 797–811.
- (52) Trodler, P.; Pleiss, J. Modeling Structure and Flexibility of *Candida Antarctica* Lipase B in Organic Solvents. *BMC Struct. Biol.* **2008**, *8*.
- (53) Torres, S.; Castro, G. R. Non-Aqueous Biocatalysis in Homogeneous Solvent Systems. *Food Technol. Biotechnol.* **2004**, *42*, 271–277.
- (54) Halling, P. J. What Can We Learn by Studying Enzymes in Non-Aqueous Media? *Philos. Trans. R. Soc. London, Ser. B* **2004**, *359*, 1287–1297.